Silver-hydrogen interactions in crystalline silicon

N. Yarykin*
Institute of Microelectronics Technology RAS, 142432 Chernogolovka, Moscow Region, Russia

J.-U. Sachse†
Max-Planck-Institut für Festköperforschung, Heisenbergstraße 1, D-70569 Stuttgart, Germany

H. Lemke
TU Berlin, Institut für Werkstoffe der Elektrotechnik, Jebensstraße 1, D-10623 Berlin, Germany

J. Weber
Max-Planck-Institut für Festkörperforschung, Heisenbergstraße 1, D-70569 Stuttgart, Germany
(Received 31 August 1998)

The creation of defects by hydrogen in silver-doped silicon crystals is investigated by deep-level transient spectroscopy. The electrical activity of the substitutional silver impurities can be totally removed due to defect formation with hydrogen atoms. However, this process includes the creation of intermediate electrically active silver-hydrogen complexes. One of the defects, Ag-H_1, contains one hydrogen atom and introduces three levels in the energy gap. Another electrically active complex is formed by addition of a second hydrogen atom to the Ag-H_1 defect. The Ag-H complexes are stable up to 300–350 °C. The electrically inactive complex includes at least three hydrogen atoms and anneals out at ~450 °C. The kinetics of the defect transformations are studied in detail, and the distance of silver-hydrogen interaction is estimated to be very close to the lattice parameter. [S0163-1829(99)02308-5]

I. INTRODUCTION

The study of hydrogen interacting with substitutional transition-metal (TM) impurities in Si has led already to the identification of electrically active hydrogen-related defects for Au,[1–3] Pt,[4,5] and Pd.[6] In this paper we present data on the formation of hydrogen complexes with Ag, which is the isoelectronic analog of gold. Therefore, the comparison of these two impurities should reveal similarities of the corresponding TM-hydrogen defects. The study of the Ag-H interaction also has practical implications because silver is used for metallization in integrated circuit fabrication, and the incorporation of hydrogen is practically inevitable during device processing.

The literature on the electrical properties of silver in silicon is rather limited.[7–10] This is explained by the very high diffusion temperature, which is needed to obtain a noticeable concentration of electrically active silver.[10] The available data for the electrical activity of Ag always give two deep levels: an acceptor level near the middle of the gap, and a donor level 0.34–0.40 eV above the top of the valence band. These levels are very similar to the energy levels of gold, and are commonly attributed to the isolated substitutional silver atom. The origin of the acceptor and donor levels in Au-doped samples was clearly related to substitutional Au.[11]

There are only a few reports on the formation of silver-hydrogen-related defects in silicon. Pearton and Tavendale were the first who subjected Ag-doped *p-n* junctions to a hydrogen plasma.[12] Both substitutional Ag levels disappeared after a plasma treatment for 2 h at 300 °C. Other authors reported that the annealing of Schottky diodes prepared on silver-doped silicon at moderate temperatures resulted in the decrease of both the silver donor[8] and acceptor[13] level concentrations in the near-surface region. Since the procedure of the Schottky-diode preparation included chemical etching, the changes observed have been ascribed to hydrogen passivation of the silver levels. Additional deep levels, which appeared after thermal annealing, were tentatively associated with electrically active silver-hydrogen complexes.[8]

The present paper gives a systematic deep-level-transient-spectroscopy (DLTS) study of the interaction of hydrogen with silver in silicon. It is shown that the electrical activity of silver can be fully passivated by hydrogen. However, the process of passivation includes the formation of intermediate silver-hydrogen complexes, which are electrically active. Based on the spatial distribution and formation kinetics, energy levels observed after hydrogenation are assigned to different silver-hydrogen complexes. Preliminary results of our study were already published in Ref. 14.

II. EXPERIMENT

A. Samples

Silicon single crystals were doped with silver during the floating-zone growth process.[15] The crystals were codoped with phosphorus ($[P]=2\times10^{14}\,\mathrm{cm}^{-3}$) or boron ($[B]=1.5\times10^{14}\,\mathrm{cm}^{-3}$). Samples were cut from two different *n*-type crystals, which differed by the cooling rates after crystal growth (type I: 10 K/s, type II: 1 K/s). In all samples the concentration of the electrically active Ag atoms is ~15% of the shallow dopant concentration.

The hydrogenation of the samples was performed during wet chemical etching in the acid solution $HF:HNO_3:CH_3COOH$ (1:2:1) at ambient temperatures. The

etching rate is about 20 μm/min. The Schottky contacts of 2-mm diameter were fabricated by vacuum metal evaporation at room temperature with Au on *n*-type samples and Al on *p*-type samples. Ohmic contacts were produced by scratching the back side of the samples with an eutectic InGa alloy.

Some chemically etched samples were annealed at temperatures between 200 and 500 °C for 1 h in an Ar atmosphere. No additional surface treatment was performed in this case before Schottky diode fabrication.

B. Measurements

The measurements were performed on a computerized DLTS system. The lock-in amplifier provided the sine-wave correlation. If not indicated otherwise, the lock-in frequency was set to 18 Hz. Activation energies and capture cross sections of the defects are determined from the Arrhenius plot of the emission rates, using the standard T^2 correction. In addition, we determined the capture cross section of most levels by the variation of the filling pulse width. Generally, the temperature dependence of the emission rate was extracted from the DLTS maximum position at different lock-in frequencies. However, for strongly overlapping DLTS peaks, the capacitance (C-t) transients were recorded at different temperatures near the maxima of these peaks, and the emission rates were obtained from a deconvolution of the transients into two exponential decays. To improve the accuracy of the emission rate calculation, the transients were recorded from the regions, which were located at different depths and had different ratios of the overlapping peak amplitudes. Then the deconvolution was performed under the assumption that the emission rates did not change with depth. The effect of electric field on the carrier emission rate was investigated by the double DLTS (DDLTS) technique, so that the emission from the same (usually near surface) region was measured at different reverse biases.

The spatial distribution of the deep-level centers was calculated by digital differentiation of the DLTS signal dependence on the filling pulse amplitude at a fixed reverse bias. The inhomogeneous profile of the shallow dopants, which was determined from the CV measurements, was properly included in the evaluation of the deep-level defect concentration. In the case of overlapping peaks the interference of the DLTS signals, which arise from different centers, was also taken into account during the profile calculation.

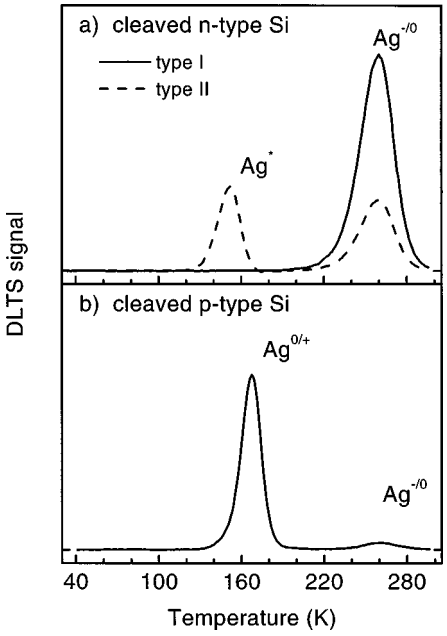

FIG. 1. DLTS spectra from cleaved Ag-doped samples. (a) *n*-type Si. (b) *p*-type Si. Type-I samples were cooled faster after crystal growth (10 K/s) compared to type-II samples (1 K/s). ($\nu_e = 42\,s^{-1}$, $t_f = 1$ ms, $V_r = -2$ V, and $V_p = 0$ V).

III. RESULTS

A. Cleaved samples

Typical DLTS spectra of cleaved, Ag-doped samples are given in Fig. 1. In Fig. 1(a), spectra are shown for the two different *n*-type Si samples, which were cooled differently after growth. The type-I sample, which was cooled faster, shows only the $Ag^{-/0}$ acceptor level ($E1{:}E_C - 0.55$ eV) of substitutional Ag. We will keep the original labeling of the

TABLE I. Energy levels, majority carrier capture cross sections, and assignment of the deep levels observed in silver-doped silicon.

Level	Activation energy E_A (eV)	σ_∞[a] (10^{-15} cm^2)	σ[b] (10^{-15} cm^2)	Assignment
$Ag^{-/0}(E1)$	E_C-0.55	7.5	0.12	Silver acceptor
$E2$	E_C-0.45	0.24		$(Ag\text{-}H)^{-/0}$
$E3$	E_C-0.09	0.67	0.0019[c]	$(Ag\text{-}H)^{=/-}$
$E6$[d]	E_C-0.5			$(Ag\text{-}H_2)^{-/0}$
Ag*($E4$)	E_C-0.30	1.3		(Ag-Ag) (Ref. 15)
$E5$	E_C-0.46	1.7		(Ag*-H)
$Ag^{0/+}(H1)$	E_V+0.37	97	3.8	Silver donor
$H2$	E_V+0.28	6.6	2.5	$(Ag\text{-}H)^{0/+}$
$H3$	E_V+0.38	2.1	0.66	$(Ag\text{-}H_2)^{0/+}$

[a]From extrapolation of the Arrhenius plot.
[b]From variation of the filling pulse width.
[c]Temperature dependent. The value at 52 K is given.
[d]Only indirect evidence exists for this level.

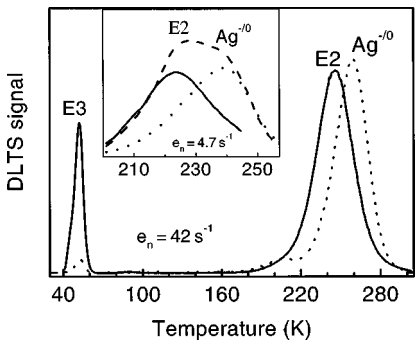

FIG. 2. DLTS spectra of the *n*-type (I) silver-doped sample measured after chemical etching in the near-surface region (solid line) and deeper in the crystal bulk (dotted line). Spectra in the inset were taken at much lower lock-in frequency. Both $E2$ and $Ag^{-/0}$ centers contribute to the DLTS signal at intermediate depth (dashed curve).

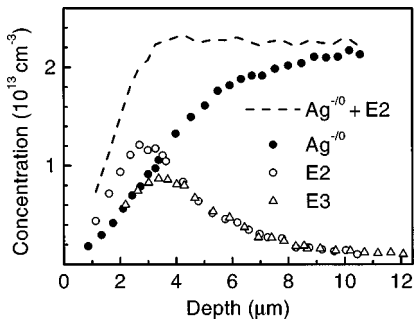

FIG. 3. Depth profiles of the defects observed in *n*-type (I) crystal after chemical etching. The dashed line represents the sum concentration of the $Ag^{-/0}$ and $E2$ centers.

hydrogen-induced levels which was proposed in Ref. 14, but for the original substitutional Ag levels we will use in this manuscript the donor or acceptor assignment $Ag^{0/+}$, $Ag^{-/0}$, etc. An additional level Ag*, which was originally labeled $E4$ at $E_C - 0.30$ eV, was detected only in the type-II samples. For both the $Ag^{-/0}$ and Ag* levels we find a homogeneous distribution into the bulk. The origin of the corresponding center for the Ag* level is still under discussion, but a similar DLTS peak was reported in several publications on Ag-doped Si.[7–9,16] Lemke[17,18] studied the thermal stability of the Ag* level: at around 600 °C, Ag* fully transforms into substitutional Ag, and an interstitial-substitutional Ag-Ag pair was proposed to explain the thermal properties of Ag*. In *p*-type samples, the $Ag^{0/+}$ donor (labeled $H1$ in Ref. 14) of substitutional Ag ($E_v + 0.37$ eV) is the only dominant trap in the type-I and -II samples [Fig. 1(b)]. However, the concentration of the Ag levels was found to be reduced by a factor of 2–5 in the type-II samples. A peak at ~260 K (too small for an accurate determination of the activation energy) was found in the DLTS spectra of all silver-doped *p*-type samples. The peak position is the same as for the $Ag^{-/0}$ level in *n*-type crystals. Therefore, we believe that this peak is caused by the process of partial filling with electrons of the $Ag^{-/0}$ level in the space-charge region. Considering the transitions from this level both to the valence and conduction bands, it is easy to show that the filling rate is determined by the faster transition to the conduction band. A very similar transition is found in Au-doped samples.[2,19]

The interpretation that the $Ag^{0/+}$ donor and the $Ag^{-/0}$ acceptor belong to the same substitutional Ag defect was recently questioned in Ref. 16. From our measurements on *n*- and *p*-type samples, we have no support for two different Ag defects, all our results can be explained with only one substitutional Ag center which has donor and acceptor levels.

The level position and capture cross section of the substitutional Ag levels and the Ag* level are given in Table I. Note the extremely high value of the hole capture cross section which was determined from the extrapolation of the Arrhenius plot for the $Ag^{0/+}$ level. In contrast, we have measured this parameter also by varying the filling pulse width and got an approximately 30 times lower value. The same property of the capture cross section was found for the silver acceptor level. This behavior was reported already in Ref. 9, but is not understood.

B. Chemically etched *n*-type samples

1. DLTS spectra of n-type (I) crystals

The DLTS spectra from *n*-type (I) Ag-doped crystals after chemical etching are shown in Fig. 2. The dotted curve was measured with a high reverse bias (20 V) and a small filling pulse amplitude (5 V). Under these conditions only the centers located at greater depths (~8–11 μm) contribute to the DLTS signal. The deep-level spectrum is very similar to that of cleaved samples. The activation energy and capture cross section of the peak at 258 K correspond to the silver acceptor level $Ag^{-/0}$ (see Table I). A small shoulder at ~200 K can be detected, which was also reported in many previous publications on silver-doped silicon.[8,9,13] The concentration of this defect is always small compared to that of the silver acceptor. In the present paper we will not discuss this shoulder further.

The solid curve in Fig. 2 was recorded under small reverse bias, and shows the DLTS spectrum from a layer located much closer to the etched surface (~0.5–3 μm in depth). The silver acceptor signal disappears while two peaks with similar amplitudes labeled $E2$ and $E3$ appear. Note that the $E2$ level is rather close to $Ag^{-/0}$, and DLTS measurements at intermediate depths result in an overlap of these two lines. Only the DLTS measurements made at a much lower lock-in frequency (inset in Fig. 2) reveal the simultaneous presence of both defects.

2. Spatial distribution of defect levels

The depth profiles of the levels observed in the *n*-type (I) samples are presented in Fig. 3. The silver acceptor concentration reaches the constant value known from the cleaved sample in the crystal bulk and is significantly reduced close to the etched surface. The concentrations of the $E2$ and $E3$ levels exhibit maxima at 2–4 μm, and decrease to zero in the crystal bulk and toward the surface. For greater depths the concentrations of the $E2$ and $E3$ levels coincide within the accuracy of the measurements. This indicates that $E2$ and $E3$ are two levels of the same defect. The sum of this defect and the silver acceptor concentrations is nearly constant at a depth larger than 3 μm and equals the initial concentration of

electrically active silver. This again supports the supposition that the $E2/E3$ defect is formed at the expense of the silver acceptor. Note, however, that the sum, which represents the total concentration of all silver-related levels in the upper half of the gap, is reduced at a depth <3 μm.

The apparent difference in the profiles of the $E2$ and $E3$ levels in the range of 2–4 μm is greater than the experimental error. The origin for this difference will be discussed in Sec. IV.

3. CV measurements

The CV measurements on the chemically etched Ag-doped n-type Si samples give nearly flat depth profiles for the net donor concentration from 3 to 12 μm in depth, indicating that no phosphorus passivation occurs in this region due to the chemical etching. The space-charge density calculated from the CV curves reduces from $2.0\times10^{14}\,\mathrm{cm}^{-3}$ at room temperature, down to $1.7\times10^{14}\,\mathrm{cm}^{-3}$ at 53 K. At greater depths this reduction can be easily explained by the influence of the silver acceptor. At room temperature, silver is neutral in the space-charge region, and the measured space-charge density is given only by the phosphorus concentration. Electrons captured at the silver acceptor level at 53 K cannot be emitted during the time of the measurement, and leave the defect in a negative charge state. Indeed, the difference in the CV profiles measured at 300 and 53 K is in a good agreement with the $Ag^{-/0}$ concentration determined by DLTS.

The $Ag^{-/0}$ concentration decreases toward the surface (Fig. 3). However, the reduction of the space-charge density at lower temperatures is the same in the whole region accessible with CV measurements. Therefore, we conclude that $E2$ also has acceptor character. In this case the $E2$ level (as well as $Ag^{-/0}$) is negatively charged at 53 K, and causes the compensation of the phosphorus donors in the region close to the surface. The $E3$ level is too shallow to trap electrons even at 53 K, and therefore does not affect the CV measurements.

4. Properties of the E3 level

The assignment of the $E2$ and $E3$ levels to the same defect and the acceptor character of $E2$ suggest that $E3$ is a second acceptor level. In this case, the electron capture to the $E3$ level should be affected by an electrostatic barrier. The kinetics of this capture have been studied by varying the filling pulse width. To extend the temperature range, both the standard DLTS technique and recording of capacitance transients have been used. The results show that the effective capture cross section has a strong temperature dependence, and increases by an order of magnitude in the range from 44 to 61 K. Even at 61 K the capture cross section is $\sim$100 times smaller than the value determined from the Arrhenius plots of the emission rates (see Table I). The temperature dependence of the effective capture cross section corresponds to a barrier of 35 meV for capture.

The $E3$ level shows also a strong dependence of the emission rate on the electric field. Using DDLTS technique, the electron emission from a narrow layer located near the maximum of the $E3$ level distribution has been measured under two different conditions of the electric field in the analyzed layer (0.44×10^4 and 1.9×10^4 V/cm, respectively). The activation energy of the $E3$ level measured under the low-field condition is 91 meV, and decreases to 79 meV in the case of the higher electric fields.

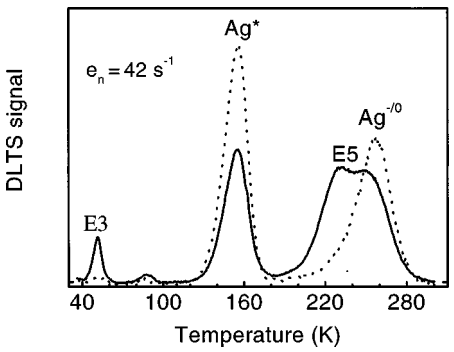

FIG. 4. DLTS spectra of n-type (II) silver-doped sample measured after chemical etching in the near surface region (solid line) and deeper in the crystal bulk (dotted line).

5. N-type (II) crystals

The deep-level spectra measured in chemically etched n-type (II) samples are shown in Fig. 4. In addition to $Ag^{-/0}$, the Ag* level is present in the bulk of the crystal in high concentrations (dotted curve). The origin of the small peak at 90 K is not known.

The solid curve in Fig. 4 demonstrates that chemical etching of the type-II samples results in the appearance of $E3$, and a new $E5$ level while the $E2$ level is hidden under the overlapping $E5$ and $Ag^{-/0}$ peaks. The spatial distribution of the levels observed in n-type (II) crystals is shown in Fig. 5. Similar to the n-type (I) samples, the concentration of all the levels in the upper half of the gap vanishes at the surface and the sum of the Ag* and $E5$ center concentrations remains flat in a wide depth range. The latter indicates that the $E5$ center originates from the Ag* defect. Note that the presence of the Ag*/$E5$ centers shows no influence on the transformation of the $Ag^{-/0}/E3$ levels (the correct determination of the $E2$ center concentration is impossible in these samples due to the strong overlap of the DLTS peaks).

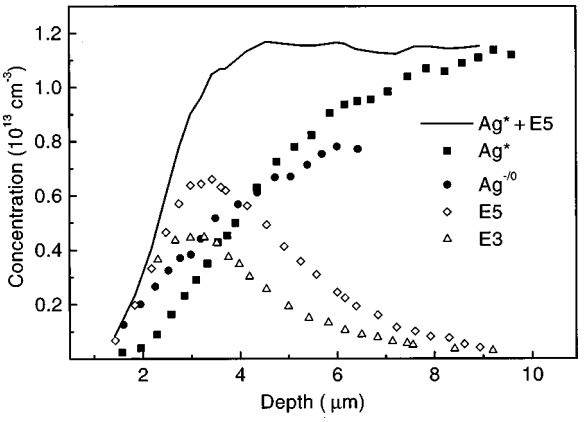

FIG. 5. Depth profiles of the defects observed in n-type (II) crystal after chemical etching. The dashed line represents the sum concentration of the Ag* and $E5$ centers.

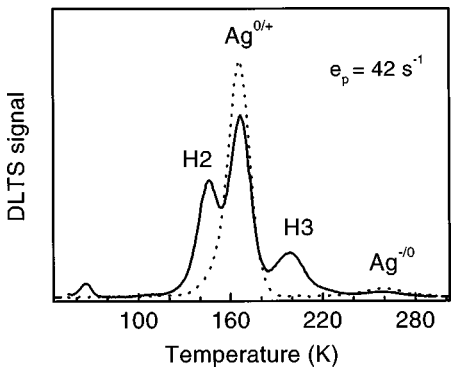

FIG. 6. DLTS curves taken in *p*-type silver-doped sample after chemical etching (dotted line) and subsequent reverse-bias annealing (RBA) for 20 min at 380 K using a reverse bias of −4 V.

C. Chemically etched *p*-type samples

1. As prepared samples

All the DLTS curves taken from *p*-type samples immediately after chemical etching show only the $Ag^{0/+}$ donor level in noticeable concentrations (Fig. 6, dotted curve). The $Ag^{0/+}$ depth profile is flat from 3.5 μm (the space-charge depth of the unbiased Schottky diode) to 15 μm (determined by the maximum voltage applied).

2. Effects of reverse-bias annealing

Chemical etching of moderately doped *p*-type silicon is known to result in a strong decrease of the active boron concentration near the etched surface due to the formation of boron-hydrogen pairs.[20] Reverse-bias annealing (RBA) injects the hydrogen atoms which are stored in the form of the H-B pairs deeper into the crystal.[21] The process of hydrogen migration can be monitored by the formation of a dip in the active boron concentration profile obtained from the *CV* measurements [Fig. 7(a)]. The kinetics of the dip formation in our samples are the same as those reported in the literature,[21] which proves that the changes observed in the net boron profile are caused by hydrogen.

The solid curve in Fig. 6 shows the DLTS signal taken after RBA at 380 K. The amplitude of the silver donor decreases, while two new peaks labeled $H2$ and $H3$ appear in the spectrum. A small peak at 65 K is only observed in a few samples, and is most probably not silver-related. Spatial distributions of the $Ag^{0/+}$, $H2$, and $H3$ centers after the RBA treatment at 380 K for 30 and 150 min, are shown in Figs. 7(b) and 7(c), respectively. The silver donor concentration follows qualitatively the *CV* profile of the shallow acceptors with a minimum approximately at the same depth as the dip in the active boron profile. At the same time, the profiles of the new defects exhibit maxima at the same depth. Moreover, the depth profile of the sum of all these three centers remains flat after the short annealing time [Fig. 7(b)]. These findings give strong arguments for the association of these new defects with two different silver-hydrogen complexes. After longer anneals the sum profile also reveals a dip in the region of the highest hydrogen concentration indicating the formation of electrically inactive complexes [Fig. 7(c)].

In all the experiments the concentration of the $H2$ level exceeds that of the $H3$ level. The concentrations of the two

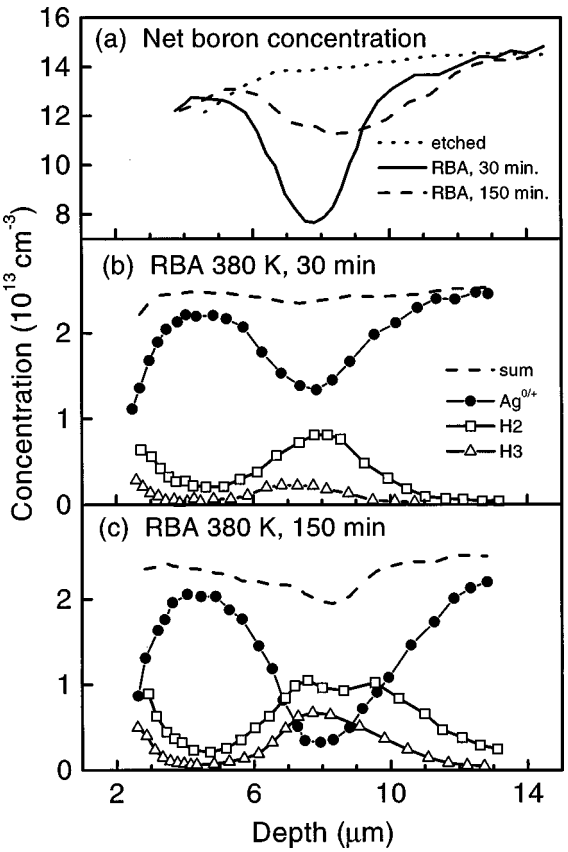

FIG. 7. Depth profiles (a) of the net acceptor concentration, and (b) and (c) deep-level defects observed in the *p*-type sample after chemical etching and reverse-bias annealing using a reverse bias of −4 V.

levels differ strongly in the region of low hydrogen concentrations and/or for shorter annealing times. Longer annealing times lead to comparable concentrations of $H2$ and $H3$. This gives a hint that the $H3$ center is formed from $H2$ by the addition of another hydrogen atom. The dip in the $H2$ defect profile in the region of the highest hydrogen concentration [Fig. 7(c)] gives another evidence for the formation of multihydrogen defects. This question will be considered in more detail in Sec. IV A.

If the annealing at 380 K is performed without applied bias or even without a Schottky diode (with subsequent evaporation of the contact), the same centers with approximately the same relative concentration as after RBA are observed by DLTS. However, the $H2$ and $H3$ centers are located near the surface in this case, and their concentration decreases rapidly towards the bulk.

The analysis (similar to that performed for *n*-type samples in Sec. III B. 3) of the *CV* profiles measured at different temperatures after long-time annealing (when all silver-related centers have comparable concentrations) allows us to determine the donor nature of the $H2$ and $H3$ centers.

3. MCTS measurements

Due to strong boron-hydrogen interaction it is not clear from the experiments on *p*-type crystals if the $H2$ and $H3$ silver-hydrogen complexes could be formed already during room temperature etching without annealing. To answer this

question minority carrier transient spectroscopy (MCTS) measurements have been performed on chemically etched *n*-type samples. The MCTS curves show that beside the $E2$ and $E3$ levels already discussed in Sec. III B, two additional MCTS signals appear at the same temperatures as expected for both the $H2$ and $H3$ levels. In *n*-type crystals the $H2$ and $H3$ center are formed already during the etching at ambient temperature and the annealing of *p*-type samples is only needed to dissociate the B-H pairs and release hydrogen.

D. High-temperature annealing

At temperatures above 200 °C the dissociation rate of the shallow dopant-hydrogen complexes (phosphorus and boron) is so fast that the diffusion of hydrogen is not influenced by the complex formation. At these temperatures the Fermi level in our moderately doped ($1.5-2\times10^{14}\,\mathrm{cm}^{-3}$) samples is located practically in the middle of the gap, independent of the type of doping, thus providing identical charge states of the defects in *n*- and *p*-type samples. Therefore, in contrast to the room-temperature etching where the hydrogen behavior is quite different in *n*- and *p*-type Si, it is expected that annealing steps at $T_{\mathrm{ann}}\geqslant200\,^{\circ}\mathrm{C}$ result in the same hydrogen distribution in both *n*- and *p*-type crystals. This allows us to make a quantitative comparison of the results obtained on the samples of different doping type. Such a heat treatment is referred to here as ''high-temperature annealing.''

Chemically etched samples of both *n*- and *p*-type have been annealed at 200–500 °C with subsequent evaporation of Schottky diodes. The most important result is that no additional deep levels with concentrations comparable to those of the silver-related centers discussed above were observed in both the upper and lower halves of the gap. Several small DLTS peaks appeared in the spectrum but were located very close to the surface. These levels seem to be related to a contamination of the samples during the anneal.

The main effect of annealing at 200 °C consists of a further (as compared to the etched samples) decrease of the silver acceptor and donor concentrations near the surface, an increase of the total amount of silver-hydrogen complexes, and a notable shift of their profiles deeper into the crystal bulk (Fig. 8). Note the excellent coincidence of the depth profiles of the $\mathrm{Ag}^{-/0}$ and $E3$ levels measured in the *n*-type sample, with those of the $\mathrm{Ag}^{0/+}$ and $H2$ levels in the *p*-type sample, respectively. This coincidence found in all the annealed samples is strong evidence that the same defect is involved in the two pairs of levels. That is, substitutional Ag for the $\mathrm{Ag}^{-/0}$ and $\mathrm{Ag}^{0/+}$ levels, and a silver-hydrogen complex for $H2$ and $E3$.

An increase of the annealing temperature up to 250–300 °C resulted in a further shift of the defect profiles deeper into the crystal as shown in Fig. 8 for the $E3$ level. This caused an expansion of the near surface region where no silver-related defects (both in *n*- and *p*-type samples) could be detected, implying that all silver atoms are involved in electrically inactive complexes.

All levels of silver-hydrogen complexes disappeared from the DLTS spectra after heat treatment at 400 °C indicating that the electrically active silver-hydrogen complexes are unstable at 400 °C. The isolated silver distribution remained similar to that after 300 °C annealing.

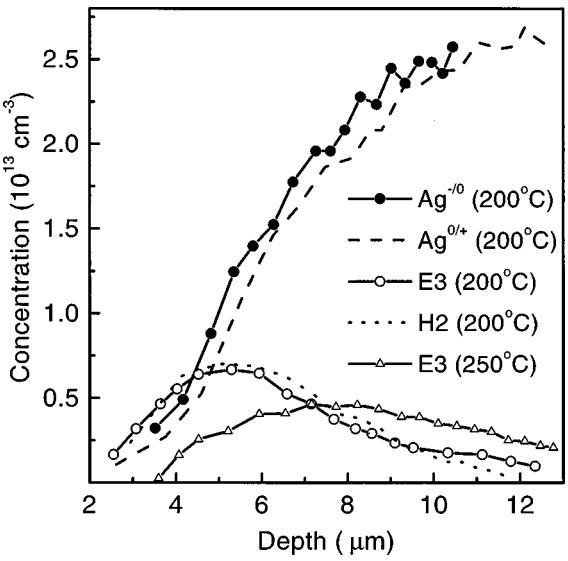

FIG. 8. Depth profiles of the silver acceptor and donor levels and silver-hydrogen complexes found after annealing of chemically etched samples at 200 and 250 °C. The electron ($\mathrm{Ag}^{-/0}$ and $E3$) and hole ($\mathrm{Ag}^{0/+}$ and $H2$) traps were measured in *n*- and *p*-type samples, respectively. For the purpose of comparison, the hole trap concentration was normalized to have the same silver concentration in the bulk of *n*- and *p*-type samples.

After anneals at 450–500 °C, the profiles of the silver acceptor and donor levels became flat, and their concentrations approached the values measured in the cleaved samples. This means that all electrically active and passive silver-hydrogen complexes anneal out completely during such heat treatments.

IV. DISCUSSION

A. Formation kinetics of Ag-H complexes during RBA procedure

The kinetics of boron passivation in our experiments agrees with the reported boron-hydrogen interaction in the literature. The transformation of substitutional silver to silver-related defects takes much more time than boron passivation. Therefore, a careful analysis of the silver related defect kinetics is necessary to prove that hydrogen is involved in these complexes.

In general, the process of successive, step by step hydrogenation of a defect can be described by the following set of equations:

$$\frac{d[N_0]}{dt}=-4\pi D r_0[N_0][H],$$

$$\frac{d[N_i]}{dt}=4\pi D(r_{i-1}[N_{i-1}]-r_i[N_i])[H],\quad i=1,2,3..., \tag{1}$$

where $[N_i]$ is the concentration of the complexes containing i hydrogen atoms, r_i the radius of hydrogen capture to the N_i complex, and $[H]$ and D the concentration and the diffusivity of atomic hydrogen, respectively. These equations imply that all the complexes are thermally stable, i.e., a hydrogen atom

once captured remains attached to the complex. This assumption is in agreement with the data of our annealing experiments (Sec. III D).

It is clear from Eq. (1) that the rate of hydrogenation depends on the hydrogen concentration, which varies with depth. For comparison of the results at different depth we rewrite Eq. (1) as

$$\left\{ \begin{array}{l} \dfrac{d[N_0]}{d\Phi} = -r_0[N_0] \\ \dfrac{d[N_i]}{d\Phi} = r_{i-1}[N_{i-1}] - r_i[N_i] \end{array} \right\}, \quad i = 1,2,3... \qquad (2)$$

with

$$\Phi = \int_0^t 4\pi D[H]dt \qquad (3)$$

as a local (dependent on hydrogen concentration) annealing time. The solution of Eq. (2) is straightforward and the problem is reduced to the calculation of the Φ value.

The distribution of hydrogen in *p*-type samples can be monitored through the passivation of boron. At any moment, most of the hydrogen is trapped by boron,[21] and only a small part is mobile and can interact with other defects. Under these conditions the concentration of mobile hydrogen can be found as

$$[H] = \frac{\nu_{\mathrm{BH}}}{4\pi D r_{\mathrm{BH}}} \frac{B_0 - [B]}{[B]}, \qquad (4)$$

where ν_{BH} and r_{BH} are the dissociation rate of B-H, pairs and the radius of hydrogen capture to boron, respectively, $[B]$ is the concentration of electrically active boron, and B_0 is the initial boron doping. It was found in Ref. 21 that $r_{\mathrm{BH}} = 4$ nm and $\nu_{\mathrm{BH}} = 3 \times 10^{-3}\ \mathrm{s}^{-1}$ at 380 K. It is important that substitution of Eq. (4) into Eq. (3) removes the unknown diffusivity D from the equations, and the absolute value of Φ can be calculated from the experimental data.

Chemically etched *p*-type samples with evaporated Schottky contacts were subjected to isothermal anneals at 380 K for 10 min to several hours with constant reverse-bias applied. Depth profiles similar to those shown in Figs. 7(b) and 7(c) were determined. The *CV* profiles of the electrically active boron were then used to calculate Φ in the depth range from 4 to 13 μm after each annealing step (it is supposed that $[B]$ needed for calculation of integral Eq. (3) was linearly dependent on the time between the measurements). These calculated values of Φ define the x values in Fig. 9. The concentrations of the $Ag^{0/+}$, $H2$, and $H3$ centers are determined by the usual DLTS profiling. The curves in Fig. 9 were calculated from Eq. (2) for the initial (nonhydrogenated) defect N_0 and the complexes containing 1 and 2 hydrogen atoms. The radii r_0, r_1, and r_2 in Eq. (2) are considered as free parameters to give the best fit to the points.

The calculated curves reflect in detail the properties of the experimental data, such as the monotonic decay of the isolated silver concentration, the decrease of the $H2$ center concentration at longer annealing time, and the slower appearance of the $H3$ defect in comparison to the $H2$ defect at shorter annealing times.

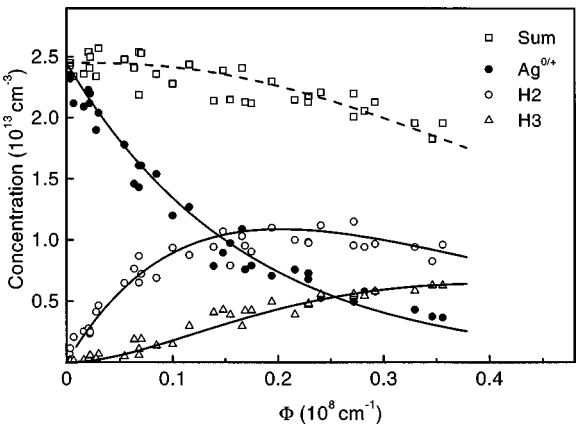

FIG. 9. Kinetics of the defect transformation in *p*-type silver-doped sample during reverse-bias annealing at 380 K. The value Φ was calculated using the *CV* profiles of the active boron concentration (see text).

In our analysis we use the hydrogen concentration, which is derived from the well-known boron-hydrogen interaction. With this hydrogen concentration we are able to fit the experimentally measured formation kinetics of the silver-related defects. This quantitative description of the kinetics is strong support of our model of the $H2$ and $H3$ centers, as being the silver-hydrogen complexes containing one and two hydrogen atoms.

For longer annealing times at 380 K the sum concentration of all silver-related deep-level centers decreases [this is seen also as dip on the dashed curve in Fig. 7(c)]. It implies that during further hydrogenation the silver atoms are transformed into electrically inactive complexes ($\mathrm{Ag\text{-}H}_x$, $X \geqslant 3$).

The curves in Fig. 9 are calculated using the values of 0.6, 0.4, and 0.5 nm for r_0, r_1, and r_2, respectively. However, due to the scatter of the data points the values of the radii cannot be precisely derived. Values around 0.5 nm are in agreement with a short-range defect-hydrogen interaction that is expected for neutral (in the space-charge region) silver atoms and silver-hydrogen complexes.

B. Depth profiles in *n*-type chemically etched samples

In this section an analysis of the depth profiles in chemically etched samples is given, which will clarify the hydrogen passivation of the Ag and Ag* center, and gives information about the diffusion parameters of hydrogen. The distinctive feature of hydrogenation during chemical etching is the steady rate of material removal. After a certain etching time a stationary distribution of the defects near the etched surface is achieved.[22] The initial concentration of a defect which is uniformly distributed over the crystal is N_0. The part $A = [N]/N_0$ of the defects which remains nonhydrogenated during chemical etching is determined by the equation

$$V\frac{dA}{dx} - 4\pi D r [H] A = 0, \qquad (5)$$

where $[H]$ and D are the concentration and diffusivity of atomic hydrogen, respectively, r the radius of hydrogen capture to the defect, and V the etching rate. Note that x is the distance from the surface which is moving during etching. It

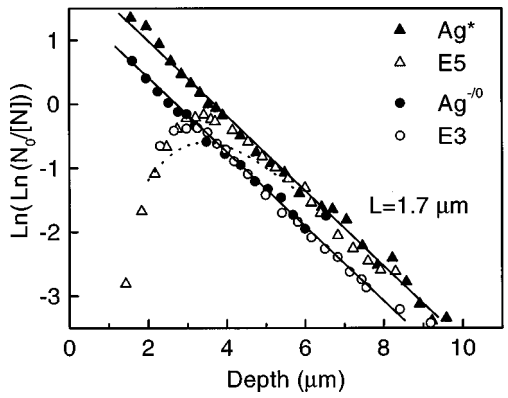

FIG. 10. Depth profiles of the deep-level defects in the *n*-type (II) chemically etched crystal. Solid lines represent the solution of Eq. (8). For the $E3$ and $E5$ defects the difference $N_0-[N]$ was used instead of $[N]$ on the y axis.

was shown earlier (see, e.g., Ref. 23) that a quasistationary distribution of mobile hydrogen atoms $[H]$ during etching is given by

$$[H]=H_0\exp(-x/L). \tag{6}$$

Here L is determined by the diffusion length of the atomic hydrogen and the etching rate

$$\frac{1}{L}=\left[\frac{1}{D\tau}+\left(\frac{V}{2D}\right)^2\right]^{1/2}+\frac{V}{2D}, \tag{7}$$

and τ is the lifetime of mobile hydrogen atoms before capture. Substitution of Eq. (6) into Eq. (5) gives the solution in the form

$$A=\exp(-4\pi rDH_0LV^{-1}e^{-x/L}). \tag{8}$$

Note that the simple exponential distribution (6) can be used only in *n*-type crystals, where τ seems to be not influenced by hydrogen penetration. In *p*-type silicon τ is initially very small, and determined by the capture to boron. During hydrogenation most of boron is transformed to the boron-hydrogen pairs, and the lifetime of mobile hydrogen increases significantly.

The depth profiles of the $Ag^{-/0}$ and Ag* levels have been measured in the same *n*-type (II) sample, and are plotted in Fig. 10. The scales in this figure are chosen so that any solution of Eq. (8) is presented by a straight line. It is seen that the $Ag^{-/0}$ and Ag* concentrations follow this dependence very well in the whole region where they can be measured. This is a strong experimental evidence to justify the use of Eq. (6). Another important point in Fig. 10 is the identical characteristic length L (the same slope in the figure) for the $Ag^{-/0}$ and Ag* centers. This behavior confirms that the passivation of the centers results from the same agent, i.e., hydrogen. In accordance with the above theoretical consideration, L is the characteristic length of the atomic hydrogen distribution. Its value is 1.7 μm in the example of Fig. 10, but can vary in the range of 1.5–2.3 μm which can be attributed to small differences in the temperature of the etching solution and to variations of the number of hydrogen traps in different samples. Note that in spite of $\sim$ 5 times difference in the etching rates used, practically the same values of L were found in the measurements of radiation defects[23] and gold[24] passivation. This strongly argues that L does not depend on the etching rate in the range studied, and the value of 1–2.5 μm is the true diffusion length $L\sim\sqrt{D\tau}$ of atomic hydrogen before its capture by the trap from which it is not released at room temperature.

The determination of L allows us to estimate the hydrogen diffusivity at room temperature. Solving Eq. (7) with respect to D, and substituting the known values of V and L, we obtain $D\geqslant 5\times10^{-9}\,\mathrm{cm^2\,s^{-1}}$. This value of D is more than two orders of magnitude higher than the one extrapolated from high-temperature measurements.[25] However, the diffusivity of hydrogen determined from our experiments could be different from the diffusivity determined under thermal equilibrium. Chemical reactions on the surface and also light shining onto the sample during etching are possible sources for nonequilibrium conditions.

The only parameter, which accounts for the particular trapping center in Eq. (8) is the radius r for the hydrogen capture. The shift of the two lines in Fig. 10 indicates that the radius of the hydrogen capture to the Ag* center is approximately 1.8 times larger than that to the silver acceptor. The absolute values for r depend on H_0, which is not known from experiment. However r cannot exceed $\sim$1 nm because the hydrogen diffusion length determined by the capture to the silver atom cannot be smaller than the experimentally measured L. If one accepts the value of $r\approx0.3-0.5$ nm (this value was derived for hydrogen pairing with silver in Sec. IV A, and with the vacancy-oxygen complex in Ref. 23), and takes into account the estimated value of D from above, we find $H_0\leqslant10^{15}\,\mathrm{cm^{-3}}$.

The concentrations of the hydrogen-related $E3$ and $E5$ centers are also shown in Fig. 10. Note that N was replaced by N_0-N for the y axis in this case. The data follow at larger depth the profiles for Ag and Ag*, verifying again that Ag/$E3$ and Ag*/$E5$ are closely related defects. Nearer to the surface, the points for the $E3$ and $E5$ centers reveal a decrease down due to the formation of complexes containing more hydrogen atoms. The calculated profile of the $E5$ centers is shown in Fig. 10 by the dotted curve, where the radius of the hydrogen capture to the $E5$ center is chosen to give a good fit to the $E5$ profile maximum. In the range from 2.5 to 4.5 μm, the experimentally determined concentration of $E5$ exceeds the calculated one. In Sec. IV C we will show that this behavior can be explained by another Ag-H defect, which was up to now not accounted for.

C. Comparison with gold-doped crystals

The substitutional impurities, silver and gold in silicon, both reveal amphoteric behavior. The energy levels in the hydrogenated gold-doped silicon[1–3] nicely resemble the levels for the Ag-H complexes (Fig. 11). Note that not only is the number of levels the same, but the level positions of the different TM-H complexes are very similar. Such a behavior for the hydrogen complexes is astonishing, but is a consequence of the intuitive vacancy model for substitutional transition metals which was proposed by Watkins.[26] The agreement between the Ag and Au-related levels gives confidence in our interpretation of the results both on silver and gold. For example, the $E2/E3$ and $G4/G1$ pairs are both attributed to the first and second acceptor levels of the complexes con-

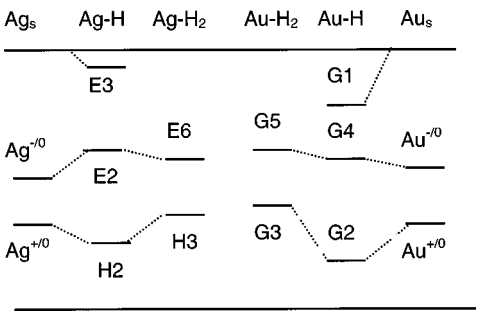

FIG. 11. Schematic diagram of the energy levels ascribed to the different silver-hydrogen (present paper) and gold-hydrogen complexes (Refs. 1–3).

taining one hydrogen atom in silver- and gold-doped crystals, respectively. The double-acceptor nature of the $E3$ level is experimentally supported by the small, temperature-dependent capture cross section. In the Au case, the capture of the second electron to the $G1$ level was detected.[3] Another example, the $G4$ level of the gold-hydrogen complex, is practically coincident with the gold acceptor level and only recently the two levels were resolved by high resolution (Laplace) DLTS.[27]

The comparison of the complexes with more hydrogen atoms leads to the following correlation and assignments. The $G3$ level was found to arise in gold-doped silicon as a result of hydrogenation. However, its formation and the number of hydrogen atoms involved in the complex are not understood. Based on the resemblance with the $H3$ level, the $G3$ level appears to belong to the Au-H_2 defect. Some peculiarities in the annealing kinetics and the small concentration compared to the Ag-H_2 complex are related to the lower thermal stability of the Au-H_2 complex. The interesting question remains about other energy levels of the TM-H_2 complex. We have already noted the surprising difference in the concentration of the $E2$ and $E3$ levels in the near surface region (Fig. 3). The comparison with gold-doped samples gives further confidence in our identification of the two levels belonging to the same Ag-H_1 center. Therefore, the difference in concentration should be ascribed to another defect with its level located near the silver acceptor ($E6$ in Fig. 11). The depth distribution of this defect (derived as the difference between the $E2$ and $E3$ profiles in Fig. 3) is in agreement with the assumption that the complex contains more than one hydrogen atom. At a similar energy position another defect level ($G5$ in Fig. 11) was detected in the hydrogenated gold doped silicon and attributed to a gold-hydrogen complex with more hydrogen atoms than the $G1$ defect.[3]

In spite of the great similarities in the position of their energy levels, a pronounced remarkable difference should be noted in the thermal stability of the silver-hydrogen and gold-hydrogen complexes, and their depth profiles after annealing. The $G1$ defect is distributed almost uniformly over the region of several micrometers adjacent to the etched surface after annealing at 150–200 °C.[1] The distribution of the Ag-H complexes is always more confined to the near-surface layer. However, the Ag-H complexes are more stable and disappear only after 400–500 °C annealing vs 250–300 °C for the Au-H defects.

Very recently, *ab initio* calculations of the structure and level positions of several TM-H complexes (TM=Ag, Au, Pd, Pt) have been performed.[28,29] These calculations confirm the similarities in the energy level structure of isoelectronic complexes, and give also good quantitative agreement with the experimental values. Three energy levels were calculated for the Au-H_1 and Ag-H_1 complexes. Other calculated levels can be associated with the $G3/G5$ and $H3/E6$ levels in Au- and Ag-doped samples. The calculations predict, for the Ag-H_3 and Au-H_3 complexes, a single acceptor level close to the conduction band. Our experiments give no evidence for any electrical activity of the TM-H_3 defects. An acceptor level with binding energy larger than 100 meV should be easily detectable in our experiments. The general agreement, however, between the calculated and the experimental levels of the various Ag-H and Au-H complexes strongly supports our identification of the levels and the number of hydrogen atoms involved in the complexes.

D. Comparison with irradiated silver-doped crystals

Recently, the effect of α-particle irradiation on the deep-level spectrum of silver-doped silicon was reported.[16,30] Two results from these publications are relevant to our study. First, the α-particle irradiation of p-type samples generated two deep-level defects, the parameters of the levels and the kinetics of their mutual transformations are very similar to those of the $H2$ and $H3$ levels found in the present work. It is suggestive to assume that these are the same defects. The authors tried to ascribe their levels to interstitial carbon and carbon-related complexes. However, we have not found any indications of C_1 (or any other defects with similar level) creation during chemical etching of silver-free samples. On the other hand, the possibility of hydrogen penetration into silicon during ion irradiation is well known.[31]

The second result from Ref. 30 is that the silver donor and acceptor levels result from different defects. This conclusion is based on the different concentration of these defects measured by the DLTS on the linearly graded p-n junctions. However, it is very important that the DLTS signals from the electron and hole traps originate in this case from the layers located at different depths. If we assume that hydrogen penetrates into the p-n junction and passivates the silver donor and acceptor levels (there are some indications for this in the discussed work), it is clear that the hydrogen concentration and therefore the silver donor and acceptor concentration can vary in different layers.

V. SUMMARY

The effect of hydrogenation during chemical etching and subsequent annealing on the energy-level spectrum of silver-doped silicon crystals was investigated by the DLTS technique. It was found in n-type crystals that all silver-related deep levels located in the hydrogen-rich near-surface region are passivated already during the etching at room temperature. Due to strong boron-hydrogen interaction in p-type crystals, the same process of silver-hydrogen interaction is much slower and takes hours at 380 K. A set of deep levels were observed to appear at the intermediate stages of passivation. Based on the quantitative analysis of the depth profiles of these levels after etching and annealing, it was established that two electrically active silver-hydrogen complexes are formed. One of these complexes contains one hydrogen

atom and introduces three energy levels in the gap. The other complex is formed by the addition of a second hydrogen atom to the Ag-H_1 complex. The electrically inactive complex presumably includes three hydrogen atoms. Based on the quantitative description of the formation kinetics, the distance of silver-hydrogen interaction is determined to be close to the lattice parameter. The observed structure of the energy levels of silver-hydrogen complexes is found to be similar to that of gold-hydrogen complexes, and to be in agreement with theoretical calculations.

ACKNOWLEDGMENTS

We thank H. J. Queisser for his interest and support. We acknowledge stimulating discussions with E. Ö. Sveinbjörnsson and A. Mesli. We are grateful to R. Jones and A. Resende for communicating theoretical results prior to publication. A. Mesli gave expert help in the MCTS experiments. The technical assistance of W. Heinz is acknowledged. N.Y. is grateful for support by the Deutsche Forschungsgemeinschaft (Contract No. 436 RUS 113/166).

*Present address: North Carolina State University, Raleigh, NC 27695-7916.

†Present address: Siemens Microelectronics Center, 01099 Dresden, Germany.

[1] E. Ö. Sveinbjörnsson and O. Engström, Appl. Phys. Lett. **61**, 2323 (1992).

[2] E. Ö. Sveinbjörnsson and O. Engström, Phys. Rev. B **52**, 4884 (1995).

[3] A. L. Parakhonskiĭ, O. V. Feklisova, S. S. Karelin, and N. A. Yarykin, Semiconductors **30**, 362 (1996).

[4] S. J. Uftring, M. Stavola, P. M. Williams, and G. D. Watkins, Phys. Rev. B **51**, 9612 (1995).

[5] J.-U. Sachse, E. Ö. Sveinbjörnsson, W. Jost, J. Weber, and H. Lemke, Phys. Rev. B **55**, 16 176 (1997).

[6] J.-U. Sachse, J. Weber, and H. Lemke, Mater. Sci. Forum **258–263**, 307 (1997).

[7] L. D. Yau and C. T. Sah, Phys. Status Solidi A **6**, 561 (1971).

[8] H. Lemke, Phys. Status Solidi A **92**, K139 (1985).

[9] N. Baber, H. G. Grimmeiss, M. Kleverman, P. Omling, and M. Zafar Iqbal, J. Appl. Phys. **62**, 2853 (1987).

[10] K. Graff, *Metal Impurities in Silicon Device Production* (Springer-Verlag, Berlin, 1994).

[11] J. W. Petersen and J. Nielsen, Appl. Phys. Lett. **56**, 1122 (1990).

[12] S. J. Pearton and A. J. Tavendale, J. Phys. C **17**, 6701 (1984).

[13] H. Feichtinger and E. Sturm, Mater. Sci. Forum **143–147**, 111 (1994).

[14] N. Yarykin, J.-U. Sachse, J. Weber, and H. Lemke, Mater. Sci. Forum **258–263**, 301 (1997).

[15] H. Lemke, in *High Purity Silicon IV*, edited by C. L. Claeys, P. Rai-Choudhury, P. Stallhofer, and J. E. Maurits (Electrochemical Society, Pennington, NJ, 1996), Vol. 96-13, p. 272

[16] A. Ali, Z. Iqbal, and N. Baber, J. Appl. Phys. **77**, 3315 (1995).

[17] H. Lemke, in *Semiconductor Silicon*, edited by H. R. Huff, W. Berholz, and K. Sumino (Electrochemical Society, Pennington, NJ, 1994), p. 695.

[18] H. Lemke, Mater. Sci. Forum **196–201**, 683 (1995).

[19] S. D. Brotherton and J. E. Lowther, Phys. Rev. Lett. **44**, 606 (1980).

[20] S. J. Pearton, J. W. Corbett, and M. Stavola, *Hydrogen in Crystalline Semiconductors* (Springer-Verlag, Berlin, 1992).

[21] T. Zundel and J. Weber, Phys. Rev. B **39**, 13 549 (1989).

[22] N. Yarykin, in *Defect and Impurity Engineered Semiconductors and Devices*, edited by S. Ashok, J. Chevallies, K. Sumino, B. L. Sopon, and W. Götz, MRS Symposia Proceedings No. 513 (Materials Research Society, Pittsburgh, 1998), p. 253.

[23] O. V. Feklisova and N. A. Yarykin, Semicond. Sci. Technol. **12**, 742 (1997).

[24] O. V. Feklisova, E. B. Yakimov, and N. A. Yarykin, Mater. Sci. Eng., B **42**, 274 (1996).

[25] A. Van Wieringen and N. Warmholtz, Physica (Amsterdam) **22**, 849 (1956).

[26] G. D. Watkins, Physica B **117&118**, 9 (1983).

[27] L. Rubaldo, A. R. Peaker, D. K. Maude, J.-C. Portal, P. Deixler, I. D. Hawkins, and J. H. Evans-Freeman, Mater. Sci. Eng., B (to be published).

[28] A. Resende, J. Goss, P. R. Briddon, S. Öberg, and R. Jones, Mater. Sci. Forum **258–263**, 295 (1997).

[29] R. Jones, A. Resende, S. Öberg, and P. R. Briddon, Mater. Sci. Eng., B (to be published).

[30] A. Ali, N Baber, and M. Zafar Iqbal, J. Appl. Phys. **77**, 5050 (1995).

[31] C. Seager, R. A. Anderson, and J. K. G. Panitz, J. Mater. Res. **2**, 96 (1987).